Detection of Printed Circuit Board Defects with Photometric Stereo and Convolutional Neural Networks

Angelika Hable
Polymer Competence Center Leoben GmbH
Roseggerstraße 12
A-8700 Leoben, Austria
angelika.hable@pccl.at

Marko Matore
Polymer Competence Center Leoben GmbH
Roseggerstraße 12
A-8700 Leoben, Austria
marko.matore@pccl.at

Anton Scherr
AT&S Austria Technologie & Systemtechnik Aktiengesellschaft
Industriepark 4
A-8350 Fehring, Austria
a.scherr@at.ats.net

Thomas Krivec
AT&S Austria Technologie & Systemtechnik Aktiengesellschaft
Fabriksgasse 13
A-8700 Leoben, Austria
t.krivec@ats.net

Dieter Gruber
Polymer Competence Center Leoben GmbH
Roseggerstraße 12
A-8700 Leoben, Austria
dieter.gruber@pccl.at

ABSTRACT

The quality inspection of printed circuit boards (PCBs) is no longer feasible by human inspectors due to accuracy requirements and the processing volume. Automated optical inspection systems must be specifically designed to meet the various inspection requirements. A photometric stereo setup is suitable for the inspection of highly reflective gold areas on PCBs. In this process, several image acquisitions are performed under different illumination directions. This can reveal defects that are not visible under other illumination systems. In this paper, we use a segmented ring light so that image acquisition is possible under four different illumination directions. Using these images, a normal map and a mean image are calculated. The defects on the gold areas of PCBs are detectable in either the normal map, the mean image, or both images. A convolutional neural network (CNN) for classification detects the defects. The input is a 6-dimensional image from normal map and mean image. An accuracy up to 95% can be achieved with the available dataset.

Keywords

Photometric stereo, printed circuit board defect detection, convolutional neural network, normal map, quality inspection

1. INTRODUCTION

It is impossible to imagine our modern world without printed circuit boards (PCBs). They are found in electronic devices and are therefore produced in very high quantities. At the same time, there are very high requirements for their quality inspection. These requirements can only be carried out by automatic inspection system, as human inspection is not possible due to the high production rates and the required accuracy of defect detection. Inspection systems for PCBs differ greatly in their scope of application. For example, there are systems for detecting missing electronic assemblies, for inspecting solder joints, and for inspecting PCB patterns. In this publication we deal with the detection of defects on gold areas (surface finish) of PCBs. This is an extension of [Hab+22]. Surface treatments have the purpose of protecting the copper from corrosion so that electronic components can later be soldered onto the copper layer. Gold coatings belong to highly reflective surfaces, thus defects can partially become visible only under certain illumination directions. One illumination approach for the inspection of highly reflective components is photometric stereo [Woo80]. In this method, at least three image acquisitions of a component are taken under different illumination directions. This allows the orientation of the surface of the component to be determined for each point [Woo80] and to create a normal image. With the obtained normal map, a trained convolutional neural network can be used to detect defects such as cracks, dents and scratches on metallic parts [Cer+20]. Another possibility is to predict the normal map using convolutional neural networks (CNNs) [Cao+22, PMM22]. In addition to the orientation of the surface normals, height information of the component surface

3D depth map can be used to detect defects. Podrekar [Pod+17] et al. use a 3D depth map for quality inspection on tablets, which is calculated from the surface normal using path integration procedure. Defects can be detected by comparing the maps with a tablet model. Curvature images can also be used to visualize defects such as scratches and wrinkles on surfaces. Curvature images are derived from the surface gradient [Ren+20]. For the detection of defects that do not have a height characteristic, 3D depth map, normal map and curvature images are not suitable. To detect these defect classes in addition to defects with height characteristics on the component surfaces, additional image information must be taken into account. Saiz [Sai+22] et al. uses several photometric images and merges them to a RGB image which is fed as input to the segmentation CNN for the detection of defects on nickel-plated components. They propose a combination of curvature images, texture images and range images (image gradient magnitude). Another method to perform quality inspection on highly reflective components is to fuse the images with different illuminations to an RGB image [LOK19]. With this method Roughness, Slope and Reflectivity [LOK19] of the component surface can be obtained. In this publication we focus on the detection of defects on the gold areas of PCBs. The defect classes include defects that are only visible through the surface normal images, defects that are only visible through a texture image and defects that can be detected in both images. For this reason, a normal map and a texture image are necessary for quality inspection. Unlike [Sai+22] and [LOK19], we do not merge both images into one RGB image, but provide the defect detection CNNs with a 6-channel image as input.

2. EXPERIMENTAL

The PCB images were acquired using an inspection setup consisting of a high resolution area scan camera, telecentric lens, segmented ring light and XY stage. Figure 1 shows the setup. The setup of the inspection system and the inspection method is described in detail in [Hab+22]. However, instead of homogeneous illumination as mentioned in [Hab+22], a white light segmented ring light (CCS HPR2-150SW-DV04M12-5) from CCS Inc. was used. With this type of illumination, certain defect classes on the highly reflective gold areas could be visualized. The individual four quadrants of this illumination can be controlled one after the other with an LSS Light Sequence Switch from CCS Inc., This allows images to be acquired from different directions of illumination. On the basis of the acquired images a photometric stereo processing is possible. The surface normals were calculated with the least mean square function of the numpy library [Har+20] from the four image acquisitions and the positions of the illuminations (light vectors).

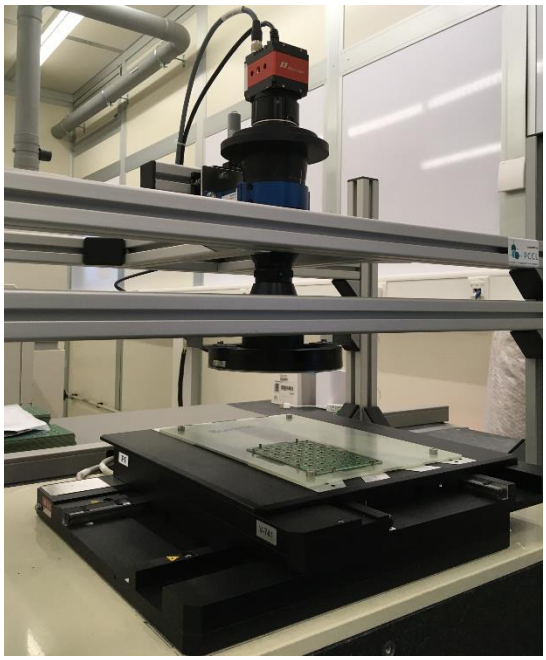

Figure 1: Inspection setup for the detection of PCB defects on gold areas. An XY stage moves the PCBs under the camera. Photometric imaging is performed with a segmented ring light and a high resolution camera so that four image acquisitions can be taken of each PCB from different illumination directions.

The light vectors are determined during the calibration of the photometric system. In this publication, we used a metal sphere and the formulas from [VW] to calculate the light vectors. In this calibration method, a metal sphere is placed under the camera and a total of 4 image captures are taken from different illumination directions using the segmented ring light. The position of the light rays directly reflected by the metal sphere can be determined by a thresholding procedure. In the case of specular reflection, the angle of reflection and the angle of observation are the same, so that the observed light intensity is equal to the incident intensity. By determining the center coordinates of the sphere, the radius and the position of the direct reflection on the sphere, the normal vector and subsequently the light vectors can be calculated using the equations in [VW]. Unfortunately, the results from the calculated light vectors showed a non-uniform normal map. This means that the color coding varies in different areas of the PCB. For a flat surface, the color coding should be the same. Despite non-uniform normal map, the defects remain visible. In addition to the normal map, a mean image is calculated from the four image acquisitions by fusing them to one RGB image using the numpy mean function.

The defects examined are copper residue, dent, contamination and discoloration. Each defect class is visible either in the normal map, in the mean image,

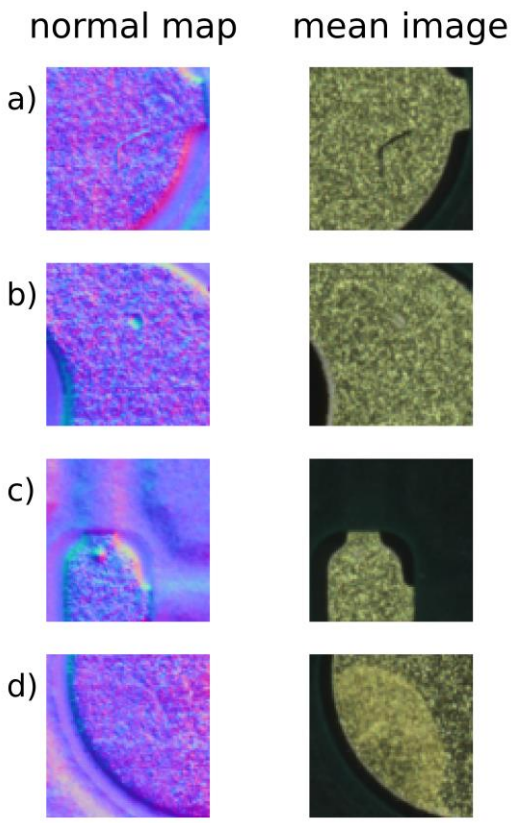

Figure 2: Defect classes displayed normal map and mean image. (a) contamination, (b) dent, (c) copper residue and (d) discoloration.

or in both images. In Figure 2 the examined defects are shown. The defect contamination is visible both in the mean image and partially in the normal map. The sliding window approach [Hab+22] is used to inspect the quality of the PCBs. Here, 100x100 patches are cut out from the normal map and mean images and are then resized to 124x124 patches and merged to a 124x124x6 dimensional image. This image is the input for the classification CNN. The output is a defect class (copper residue, dent, contamination, discoloration and OK).

3. RESULTS AND DISCUSSION

The classification CNN has a 6-dimensional image input and is composed of two consecutive convolutional layers, a batch normalization layer and a max pooling layer. At the end there are two fully connected layers with dropout layer in between. The architecture of the CNN is shown in Figure 3. Since the input consists of a 6-dimensional image (mean image and normal map), no existing network architecture such as ResNet with Transfer Learning was used, but an own network architecture was developed. Existing network architectures such as ResNet use 3-dimensional images as input. An adaptation of an existing network architecture to our needs would mean a complete training on a deep network and would be computationally more

	training	validation	test
copper residue	1083 (3249)	232	232
dent	2317 (4634)	496	495
OK	3417 (5142)	733	731
contamination	422 (5908)	90	85
discoloration	178 (3738)	38	37

Table 1: Composition of the entire dataset divided into training, validation and test dataset. The numbers indicate the amount of existing defects in the dataset. In parentheses are the number of existing data after augmentation by the augmentation algorithms.

expensive than the training of a small network from scratch. For this reason, a self-developed network architecture without transfer learning was chosen. When designing the architecture and selecting the hyperparameters such as batch size and learning rate, several training runs were performed and the network architecture and parameters were selected so that the best results in terms of accuracy and performance could be achieved. The PyTorch framework [Pas+19] was used to create the classification CNN and for training. Cross Entropy Loss, a batch size of 64, a learning rate of 0.0001 was chosen. The network was trained for 100 epochs. As optimizer the function OneCycleLR from PyTorch [Pas+19] was used. The maximum learning rate, a parameter of the optimizer, was set to 0.005.

The composition of the image data per defect is shown in Table 1. The dataset is very unbalanced. There are only few image data of the defect class discoloration while many image data of the OK class are present.

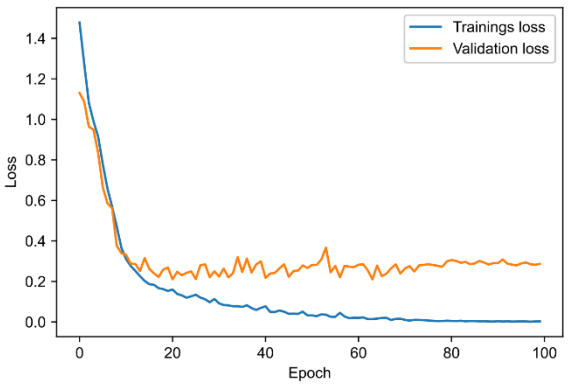

Figure 4: Training loss and validation loss when training the CNN on 100 epochs. The smallest validation loss (epoch 64) was chosen for the evaluation.

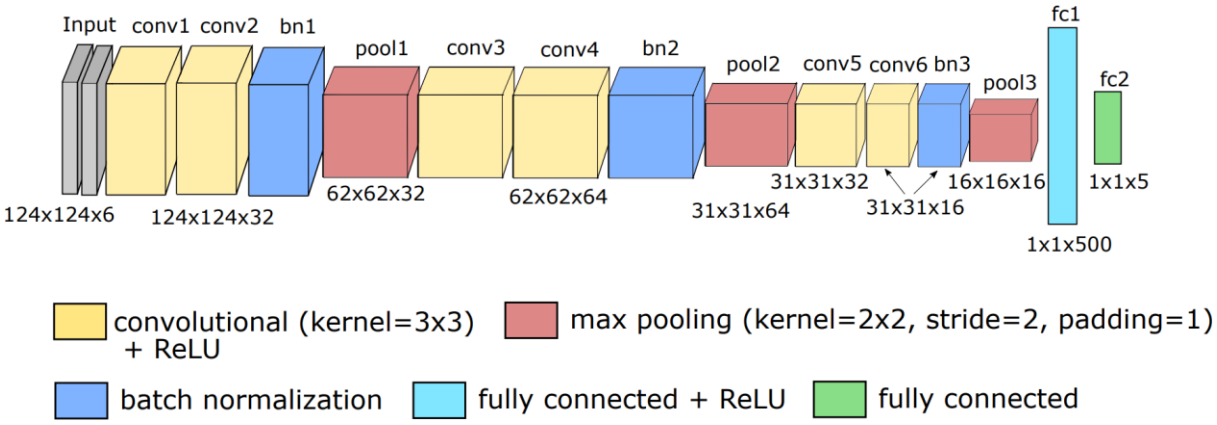

Figure 3: Network architecture of the CNN applied. The input (124x124x6) is composed of the fused mean image and normal map. The architecture structure consists of two consecutive convolutional layers, a batch normalization layer and max pooling layer. The classification is performed by two fully connected layers. The output of the last layer corresponds to the number of defect classes.

Augmentation algorithms were used to balance and augment the training dataset. All image data of the training dataset were enlarged by augmentation and for defect classes with limited data, the image data were augmented more often than, for example, image data of the OK class. For data augmentation, horizontal flips, rotations, blurring and affine transformations were performed. Furthermore, adjustments were made for brightness, contrast and intensities in the hue channel. Figure 4 shows the loss of training and validation. During training, the networks weights were saved at each epoch. For the evaluation, the network configuration of the CNN were used where the validation loss was the smallest. This was epoch 64. The results of the classification CNN are shown in Figure 5 in the form of a confusion matrix. It can be seen that the defect class discoloration provides a very good prediction accuracy, although this class has the smallest amount of image data available. Misclassification occurs especially with contamination but also with dents. These defects are mistaken for the OK class. This is possibly due to the fact that the dataset also contains difficult-to-detect contamination defects and very small expressions of the defect class dents. With this configuration, a defect detection accuracy of 95% could be achieved. The Matthews correlation coefficient (MCC) is 92%.

4. CONCLUSION

In this publication we present an inspection system for the detection of defects on the gold areas of PCBs. A photometric stereo setup is used to visualize the defects on the highly reflective gold surface and a normal map is calculated. All defects except for the defect discoloration are visible in the normal map. A mean image is calculated from the available image acquisitions, in which the defect classes discoloration and contamination are clearly visible. A classification CNN receives normal map and mean image in the form of a 6-dimensional image as input. On the test dataset an accuracy of 95% and MCC value of 92% could be achieved. One of our goals is to improve the calibration method so that a more uniform normal map can be computed. Furthermore, we want to test different input images and compare the classification accuracies.

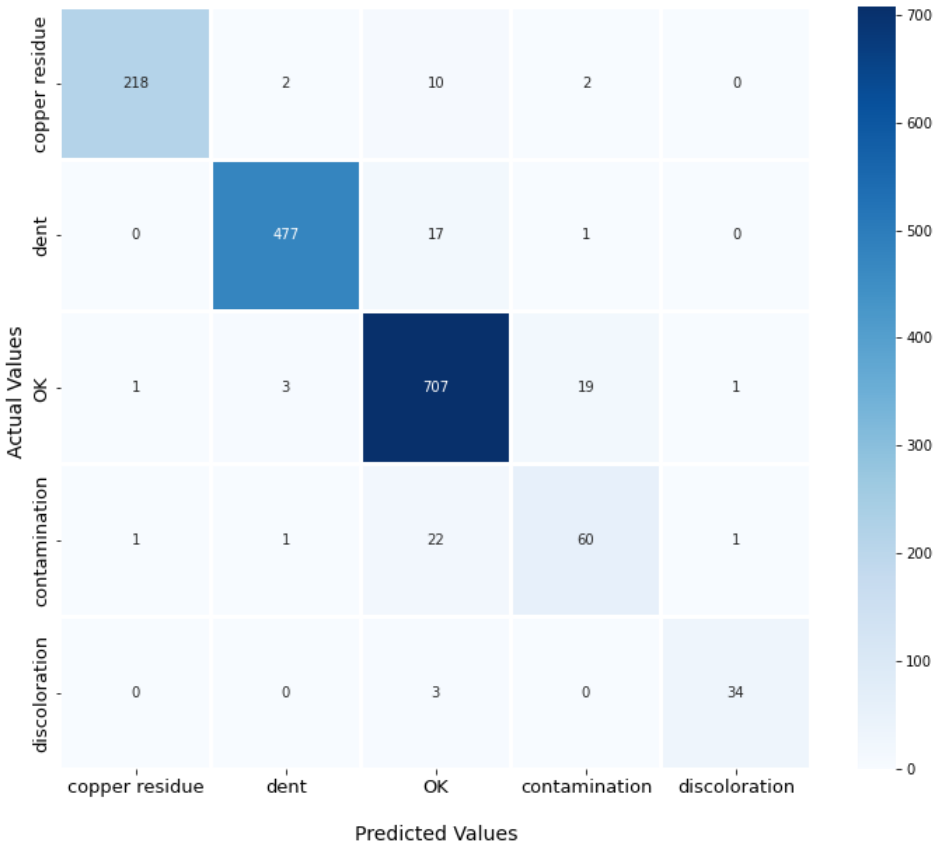

Figure 5: Confusion matrix of defect classes on the test dataset. The dataset is unbalanced. Many misclassifications occur with contamination. The best results are obtained with discoloration.

5. ACKNOWLEDGMENTS

The research work of this article was performed at the Polymer Competence Center Leoben GmbH (PCCL, Austria) within the framework of the COMET-program of the Federal Ministry for Transport, Innovation and Technology and the Federal Ministry of Digital and Economic Affairs with contributions by AT&S (Austria Technologie & Systemtechnik AG). The PCCL is funded by the Austrian Government and the State Governments of Styria, Lower Austria, and Upper Austria.

6. REFERENCES

[Cao+22] Yanlong C., Binjie, D., Jingxi, C., Wenyuan, L., Penging, G., Liuyi, H., Jiangxin, Y. Photometric-Stereo Based Defect Detection System for Metal Parts. Sensors 22.21 (2022), p. 8374. https://doi.org/10.3390/s22218374

[Cer+20] Cerezci, F., Kazan, S., Oz, M. A., Oz, C., Tasci, T., Hizal, S., Altay, C. Online metallic surface defect detection using deep learning. Emerging Materials Research 9.4 (2020), pp. 1266–1273. https://doi.org/10.1680/jemmr.20.00197

[Hab+22] Hable, A., Tabatabai, P., Lichtenegger, H. L., Scherr, A., Krivec, T., Gruber, D. P. Detection of Printed Circuit Board Defects on ENIG and ENIPIG Surface Finishes with Convolutional Neural Networks and Evaluation of Training Parameters. Journal of Microelectronics and Electronic Packaging 19.4 (2022), pp. 123–130. https://doi.org/10.4071/imaps.1814291

[Har+20] Harris C.R. et al. Array programming with NumPy. 2020. https://doi.org/10.1038/s41586-020-2649-2.

[LOK19] Lee, J. H., Oh, H. M., & Kim, M. Y. Deep learning based 3D defect detection system using photometric stereo illumination. 2019 International Conference on Artificial Intelligence in Information and Communication (ICAIIC). IEEE. 2019, pp. 484– 487. https://doi.org/10.1109/ICAIIC.2019.8669005

[Pas+19] Paszke, A. et al. PyTorch: An Imperative Style, High-Performance Deep Learning Library. Advances in Neural Information Processing Systems 32. Curran Associates, Inc., 2019, pp. 8024–8035. URL: http://papers.neurips.cc/paper/9015-pytorch-an-imperative-style-high-performance-deep-learning-library.pdf

[PMM22] Pourmand, S., Merillou, N., Merillou, S. Depth Completion for Close-Range Specular Objects. WSCG 2022: full papers proceedings: 30. International Conference in Central Europe on Computer Graphics, Visualization and Computer Vision, p. 135-141. https://www.doi.org/10.24132/CSRN.3201.17

[Pod+17] Podrekar, G., Tomaževič, D., Likar, B., Usenik, P. Model based visual inspection of pharmaceutical tablets with photometric stereo. In: 2017 Fifteenth IAPR International Conference on Machine Vision Applications (MVA). IEEE. 2017, pp. 133–136. https://doi.org/10.23919/MVA.2017.7986819

[Ren+20] Ren, X., Wang, W., Ren, J., Mao, X., Zhang, M. Research and application of label defect detection method based on machine vision. Journal of Physics: Conference Series. Vol. 1453. 1. IOP Publishing. 2020, p. 012084. https://www.doi.org/10.1088/1742-6596/1453/1/012084

[Sai+22] Saiz, F. A., Barandiaran, I., Arbelaiz, A., Graña, M. Photometric stereo based defect detection system for steel components manufacturing using a deep segmentation network. Sensors 22.3 (2022), p. 882. https://doi.org/10.3390/s22030882

[VW] Verma, C.S. and Wu, M.J. Photometric Stereo. URL:https://pages.cs.wisc.edu/~csverma/CS766_09/Stereo/stereo.html.

[Woo80] Woodham, R.J. Photometric method for determining surface orientation from multiple images. Optical engineering 19.1 (1980), pp. 139–144